8-29-2017

Ionization enhancement and suppression by phase-locked ultrafast pulse pairs

David B. Foote
University of Maryland at College Park, dbfoote@umd.edu

Y. Lin
University of Maryland at College Park

Liang-Wen Pi
University of Nebraska - Lincoln

Jean Marcel Ngoko Djiokap
University of Nebraska-Lincoln, jngokodjiokap2@unl.edu

Anthony F. Starace
University of Nebraska-Lincoln, astarace1@unl.edu

See next page for additional authors

Ionization enhancement and suppression by phase-locked ultrafast pulse pairs

David B. Foote,[1,2,*] Y. Lin,[3] Liang-Wen Pi,[4] J. M. Ngoko Djiokap,[4] Anthony F. Starace,[4] and W. T. Hill, III[1,2,3,†]

[1]*Joint Quantum Institute, University of Maryland, College Park, Maryland 20742, USA*

[2]*Institute for Physical Science and Technology, University of Maryland, College Park, Maryland 20742, USA*

[3]*Department of Physics, University of Maryland, College Park, Maryland 20742, USA*

[4]*Department of Physics and Astronomy, University of Nebraska, Lincoln, Nebraska 68588-0299, USA*

(Received 20 June 2017; published 29 August 2017)

We present the results of a study of ionization of Xe atoms by a pair of phase-locked pulses, which is characterized by interference produced by the twin peaks. Two types of interference are considered: ordinary optical interference, which changes the intensity of the composite pulse and thus the ion yield, and a quantum interference, in which the excited electron wave packets interfere. We use the measured Xe^+ yield as a function of the temporal delay and/or relative phase between the peaks to monitor the interferences and compare their relative strengths. We model the interference with a pulse intensity function and by calculating the ionization yield with the time-dependent Schrödinger equation. Our results provide insight into optimal control pulses generated with learning algorithms. The results also show that the relative phase between peaks of a control pulse, along with small features such as distortions and imperfections in the wings of an ideal shape, play a significant role in the control process.

DOI: 10.1103/PhysRevA.96.023425

I. INTRODUCTION

Shaped pulses are commonly used in control experiments because of their ability to steer dynamics in simple and complex systems at the quantum level. Their success is largely due to intense fields at 800 nm and the application of optimal control and pulse-shaping techniques [1–3]. With strong fields, however, *multiphoton* ionization is often either an early step in the dynamics or concomitant with the dynamics of interest. At low intensities, multiphoton ionization can be treated perturbatively [4–6], and the number of ions generated typically increases monotonically with the laser intensity. In the strong-field regime, perturbation theory breaks down, saturation sets in, new channels open up, and states shift in and out of resonance [7–11]. Despite the fact that even more exotic processes occur, e.g., above threshold ionization, there is still a tendency for the total number of ions to increase with increasing intensity. This is because ionization can now occur in the wings of the pulse at intensities lower than the peak intensity [12,13]. This monotonic increase is observed with simple pulse envelopes, e.g., transform-limited (TL) pulses. Evidently, more complex envelopes, especially those associated with phase-shaped pulses (i.e., optimal pulses), do not necessarily obey this trend because they are effective at altering dynamics, including ionization [14].

Optimal pulses often consist of a number of closely spaced peaks, each of which has a well-defined relative phase with respect to its neighbors. (Figure 2 of Ref. [15] is a specific example.) Pulse trains have been used for coherent control of a diverse array of processes, such as photoelectron angular distributions [16,17], magnetization [18], and molecular vibration and rotation [19]. At the same time, they have appeared in optimal-pulse solutions in control experiments [15,20–23]. Deconstruction of these pulses, to determine how they achieve their goals, has proven to be a difficult and arduous task. From studying the control landscape [15,24,25] to probing the role of chirp [26] to isolating specific degrees of freedom [15,24,26,27], success has been unsatisfying at best. While compelling reasons can be given on a case-by-case basis, finding a universal linchpin—or even determining if one exists—has been difficult.

The one prominent feature of optimal pulses that has received far less attention than others is the relative phase between components, presumably because of the perceived limited dynamic range (i.e., 0–2π rad). In this paper, we present the results of our study of how and why changing the relative phase in a complex pulse can have a profound effect on multiphoton ionization and by extension on controlling dynamics. Furthermore, we show that other minor features of a pulse, such as imperfections on the pulse wings or small subordinate peaks, can have a similarly substantial effect on the ionization.

To make our study quantitative and straightforward to analyze, we limit our focus to excitation by a pair of nearly identical pulses, each with a distinct carrier envelope phase (CEP). While we did not stabilize the CEP, we did lock the relative phase between the two pulses. In this paper, we will call the pair of pulses a twin-peaked pulse (TPP) and treat them as a single composite unit—a single pulse of complicated temporal structure. We will focus on only linearly polarized TPPs and define the time-dependent electric field of an ideal TPP as

$$\mathcal{E}_{\rm TPP}(\tau,\Delta\phi;t) = \mathcal{E}_0 e^{-i(\omega_0 t-\phi_1)}\left[\operatorname{sech}\left(\frac{t}{\Delta t}\right)+\operatorname{sech}\left(\frac{t-\tau}{\Delta t}\right)e^{i\Delta\phi}\right] + \text{c.c.}, \quad (1)$$

where $\mathcal{E}_0$ is the electric field amplitude of a single peak, ω_0 ($=2\pi\nu_0$) is the central frequency of the pulse spectrum, $1.76\Delta t$ is the intensity full width at half maximum (FWHM)

*dbfoote@umd.edu

†wth@umd.edu

of each peak when the peaks are well separated in time, τ is the time delay between peaks, $\Delta\phi \equiv \phi_2 - \phi_1$ is the relative phase between peaks, and $I_{\mathrm{TPP}}(\tau,\Delta\phi;t) \propto [\mathcal{E}_{\mathrm{TPP}}(\tau,\Delta\phi;t)]^2$ is the TPP intensity; ϕ_1 (ϕ_2) is the phase of the earlier (later) peak, measured relative to the peak of the pulse envelope of the earlier peak. Defining the CEP of each peak, $\theta_{1,2}$, in the usual way (relative to the peak of its own envelope) leads to

$$\phi_1 \equiv \theta_1, \phi_2 \equiv \theta_2 + \omega_0\tau \text{ and } \Delta\phi = \theta_2 - \theta_1 + \omega_0\tau. \quad (2)$$

We define the complex envelope of the TPP as

$$E_{\mathrm{TPP}} = \mathcal{E}_0\left[\mathrm{sech}\left(\frac{t}{\Delta t}\right) + \mathrm{sech}\left(\frac{t-\tau}{\Delta t}\right)e^{i\Delta\phi}\right]. \quad (3)$$

For a many-cycle pulse ($\Delta t \gg 1/\nu_0$), the envelope does not change appreciably over one optical period. In the absence of CEP stabilization, one must average $[\mathcal{E}_{\mathrm{TPP}}(\tau,\Delta\phi;t)]^2$ over all ϕ_1 to determine the intensity, which gives $I_{\mathrm{TPP}}(\tau,\Delta\phi;t) \propto |E_{\mathrm{TPP}}(\tau,\Delta\phi;t)|^2$ [28,29]. With Eq. (3), the intensity becomes

$$I_{\mathrm{TPP}}(\tau,\Delta\phi;t) = I_0\left[\mathrm{sech}^2\left(\frac{t}{\Delta t}\right) + \mathrm{sech}^2\left(\frac{t-\tau}{\Delta t}\right) + 2\mathrm{sech}\left(\frac{t}{\Delta t}\right)\mathrm{sech}\left(\frac{t-\tau}{\Delta t}\right)\cos(\Delta\phi)\right], \quad (4)$$

where $I_0 = (c\epsilon_0 n/2)\mathcal{E}_0^2$ is the single-peak intensity, ϵ_0 is the vacuum permittivity, c is the speed of light, and n is the refractive index. In what follows, we will show that the system responds fundamentally differently to Eq. (4) than it does to an isolated, transform-limited pulse.

The goal of our investigation is to explore how phase coherence can influence multiphoton ionization, rather than deciphering the dynamics of a particular controlled molecular process. Thus, to obviate the need to address additional complications associated with molecular ionization, our target was an atom, Xe. As with many molecular systems, a number of photons are required to reach the field-free ionization threshold. For Xe (with an ionization potential of 12.13 eV), eight 800-nm photons are needed to reach Xe^+.

Clearly, optical interference (OI) will play a significant role in the ionization when the peak separation of the TPP is sufficiently small, as can often be the case in optimal control pulses. In addition to the classical OI, the strength of which will depend on the fractional overlap of the peaks, a more subtle quantum beat, which we will call quantum interference (QuI) in this paper, may influence the ionization as well. For atomic ionization, there are at least three possible mechanisms through which quantum beats could arise.

Mechanism I relies on a superposition between the ground state and a bound excited state that will be established by the first peak of the TPP. This superposition will result in a population oscillation between these two states on a time scale commensurate with their energy spacing. The second pulse in the TPP interacts with the superposition. When the bandwidth of the pulses is sufficient to excite several bound excited states coherently, mechanism II results. This second mechanism is characterized by a population oscillation between the excited states with a period corresponding to the energy spacing between them. The oscillations in mechanism II have a much longer period than the oscillations in mechanism I. Mechanisms I and II can occur simultaneously. Blanchet *et al.* [30] were able to distinguish these two mechanisms in a (2+1)-photon ionization of Cs through the $7d\ ^2D_{3/2,5/2}$ states with a 150-fs TPP at 768 nm. The excited bound states were reached by a two-photon transition. Detection of QuI was enabled by the absorption of an additional photon to create Cs^+. Their ion signal showed the expected modulation with about half the laser period (mechanism I, energy spacing $\simeq 2h\nu_0$, where h is Planck's constant) with a beat note commensurate with the $7d$ doublet energy spacing (mechanism II). The concomitant OI with period $1/\nu_0$ also was observed. It is interesting to note that the QuI mechanisms I and II they observed extended well outside the temporal region where OI was observed.

The third QuI (mechanism III) of interest occurs when each peak of the TPP generates a continuum electron wave packet. The wave packets necessarily interfere when they overlap spatially and temporally at the detector, causing a modulation of the photoelectron signal due to ambiguity in knowledge of which pulse was responsible for the birth of the electron. This also can be viewed as a temporal analogue to a Young's double-slit arrangement. Wollenhaupt *et al.* [31] interpreted their one-photon ionization of an incoherently prepopulated $5p$ state of K with a 790-nm fs TPP in terms of mechanism III. It turns out that the strength of mechanism III tends to follow that of OI; OI and QuI were not clearly distinguished in Ref. [31] because the modulation periods for the two are the same. The modulation period of mechanism III is $h/(E_b + E_{el})$, where E_b and E_{el} are the ionization energy from the initial state ($5p$ in the case of Ref. [31]) and the electron kinetic energy ($= nh\nu_0 - E_b$) respectively (where n is the number of photons required to ionize). For $n = 1$, OI and QuI have a period of $1/\nu_0$. For $n > 1$, the period of the corresponding modulation is n times smaller, making OI and QuI distinguishable. Thus, in atomic Xe a modulation due to QuI mechanism III involving ground-state ionization would have a period of $1/(8\nu_0)$.

While there are no field-free intermediate resonances near 800 nm in Xe, there are states approximately 0.3 eV below and 0.2 eV above the energy corresponding to the absorption of seven photons. Depending on the field intensity, the ac-Stark effect could shift some of these states into a seven-photon resonance (Freeman resonances [10,11]), which could leave excited-state population less than 1.5 eV below the ionization threshold after the first peak. The (7+1)-photon ionization could lead to modulation of period $1/(7\nu_0)$ (mechanism I) with the possibility of much longer beat notes due to two or more intermediate states being populated coherently (mechanism II). Finally, a less direct QuI mechanism III could occur, resulting from a (7+1)-photon ionization from the first peak of the TPP and a one-photon ionization of the residual population in the excited state from the second peak. We call this mechanism III′, and it would have a period of $1/\nu_0$.

Exploring the effects of OI and QuI both experimentally and theoretically is the central theme of this paper, which is organized as follows. We describe the details of the experiment in Sec. II followed by an outline of the simulations in Sec. III. Our results are presented in Sec. IV and discussed in Sec. V.

II. EXPERIMENTAL SETUP

Twin-peaked, phase-locked pulses were prepared from single, isolated input pulses generated with a commercial femtosecond Ti:sapphire oscillator-amplifier laser system. The pulses were nearly transform limited with a FWHM of 80 fs, corresponding to $\Delta t \simeq 50$ fs in Eqs. (1) and (4) (about 30 optical cycles). The input pulses had a central wavelength $\lambda_0 = c/\nu_0 \simeq 805$ nm, a bandwidth of approximately 20 nm, and a beam divergence of approximately 1.5 times the diffraction limit. We characterized the input pulses with a self-diffraction frequency-resolved optical gating (SD-FROG) [32] and a Wizzler [33]. We generated TPPs by splitting the input pulse into two nearly identical copies in two distinct ways: (1) using a spatial light modulator-based pulse shaper (PS) [15,34] in a $4f$ arrangement and (2) using a Mach-Zehnder interferometer (MZ) with one variable arm using an Aerotech ALS130 linear motor stage. In both cases, the polarization vectors of the two peaks were aligned, which is the typical case in control experiments. We will refer to a TPP generated by the PS (MZ) approach as a $\mathrm{TPP_{PS}}$ ($\mathrm{TPP_{MZ}}$).

We employed a 128-pixel liquid crystal on silicon spatial light modulator (LCOS-SLM) [35] to create the $\mathrm{TPP_{PS}}$. Their generation requires that a mask be applied to the SLM that will imprint a spectral intensity and phase on the input pulse that is the Fourier transform of the desired $\mathrm{TPP_{PS}}$:

$$I_{\mathrm{TPP}}(\tau,\Delta\phi;\omega) = \tilde{I}_0 \mathrm{sech}^2\left(\frac{\omega-\omega_0}{\Delta\omega}\right)\cos^2\left(\frac{\omega\tau-\Delta\phi}{2}\right), \tag{5}$$

where $\Delta\omega = 2/(\pi\,\Delta t)$ and $\tilde{I}_0 = 2\pi I_0 \Delta t$. We controlled τ and $\Delta\phi$ independently by changing the mask on the SLM. We can use this approach to explore the phase-dependent response of the ionization at fixed ω_0 and τ. In the experiments, we varied $\Delta\phi$ over 3π rad in steps of $\sim\pi/4$ rad at $\tau \simeq 150$ fs (where ω_0 was fixed by the input pulse wavelength). The values for τ and $\Delta\phi$ were taken from SD-FROG measurements. The uncertainty in τ was estimated by measuring a sample $\mathrm{TPP_{PS}}$ ten times and computing the standard deviation in the fit values of τ, and it was found to be 0.66 fs. Each $\mathrm{TPP_{PS}}$ was measured once with the FROG during the experiment. The energy of the $\mathrm{TPP_{PS}}$ was fixed at 40 μJ for each step; the energy was adjusted with a combination of a rotatable half-wave plate and polarizer. Minor alignment variation and residual spatial and temporal chirp caused the energy confined to each peak of the $\mathrm{TPP_{PS}}$ to vary by about 10% as $\Delta\phi$ was tuned.

In the MZ approach, the pulse traveling in each arm was a true replica of the input pulse, so nominally $\theta_1 \simeq \theta_2$ except for small differences caused by the beam splitters and mirrors of the interferometer not being identical. It is important to note that these differences will be nearly constant throughout the experiment; i.e., $\Delta\theta \equiv \theta_2 - \theta_1$ will be fixed (observed to be constant within $\pi/10$ rad in the experiment). As a result, when ω_0 is held constant, Eq. (2) demands that $\Delta\phi$ is linear in τ ($= \Delta l/c$, where Δl is the path length difference in the arms). Nominally, we varied Δl by increments of 20 nm, which corresponds to a change in τ of 0.067 fs. The translation stage we used to change the arm length, however, made steps that varied between 0.046 and 0.102 fs (Δl between 14 and 30 nm) even with feedback control. The value of τ for a $\mathrm{TPP_{MZ}}$ was determined by fitting the fringes in the pulse spectrum to Eq. (5) and separately by a SD-FROG measurement. The uncertainty in τ was determined in the same fashion as in the PS experiment; we took 1000 measurements of a sample $\mathrm{TPP_{MZ}}$ spectrum (at $\tau = 150$ fs) and found the standard deviation in the fit value of τ to be 0.45 fs. The spectrum of each $\mathrm{TPP_{MZ}}$ during the experiment was measured only once. The uncertainty in $\delta\tau$, the change in τ between two increments of Δl, was much smaller ($\simeq$0.03 fs).

In the MZ approach, we fixed the $\mathrm{TPP_{MZ}}$ energy to 40 μJ for $\tau \gg \Delta t$. Thus, the $\mathrm{TPP_{MZ}}$ energy changed periodically as τ was varied due to OI as $\tau \to \Delta t$. The energy was not shared equally between the $\mathrm{TPP_{MZ}}$ peaks; the experiments were run with peak 2 (the later peak) having $\sim$10% less energy than peak 1. The MZ approach enables $\mathrm{TPP_{MZ}}$-induced ionization to be explored over a wider range of τ with higher temporal, and hence phase, resolution.

We performed the experiments by leaking xenon into the vacuum chamber to a pressure of $4.0(1)\times10^{-7}$ Torr, two orders of magnitude higher than the base pressure. The TPPs were focused to a spot of nominal radius ($1/e^2$ intensity) 7 μm with a concave spherical mirror ($f = 75$ mm). For our 40-μJ TPPs, this gives a nominal intensity of 3×10^{14} W/cm^2. The number of xenon ions emanating from the focal spot were measured with a time-of-flight (TOF) spectrometer having a 30-cm flight tube as described in detail in Ref. [36]. The TOF waveforms were captured by a 500-MHz digital oscilloscope (LeCroy 9350AM).

III. NUMERICAL SIMULATIONS

We performed two simulations, which are compared with the experimental results in the next section. The first simulation was a calculation of the intensity of the $\mathrm{TPP_{MZ}}$. To make the simulations as compatible with the experiment as possible, we used reconstructed input pulses from SD-FROG and Wizzler spectra. We calculated the $\mathrm{TPP_{MZ}}$ field and intensity from the reconstructed intensity and phase of the input pulse, $I(t)$ and $\phi(t)$ respectively, as follows:

$$\mathcal{E}_{\mathrm{sim}}(\tau,\Delta\phi;t) = \sqrt{\frac{2}{cn\epsilon_0}}e^{-i(\omega_0 t-\phi_1)}[\sqrt{I(t)}e^{-i\phi(t)} + \beta_{MZ}\sqrt{I(t-\tau)}e^{-i\phi(t-\tau)}e^{i\Delta\phi}] + \mathrm{c.c.}, \tag{6}$$

$$I_{\mathrm{sim}}(\tau,\Delta\phi;t) = \frac{cn\epsilon_0}{2}[\mathcal{E}_{\mathrm{sim}}(\tau,\Delta\phi;t)]^2, \tag{7}$$

where $\beta_{MZ} = 0.94$ accounts for peak 2 having less energy. We will compare the intensity in Eq. (7) with the $\mathrm{TPP_{MZ}}$ in the next section.

The second simulation involved solving the time-dependent Schrödinger equation (TDSE) to calculate the TPP-induced ionization probability. The interaction potential was produced by the field in Eq. (6) as well. We performed the TDSE calculation in momentum space where the photoelectrons have finite momenta and localized wave functions. For the calculations, we used the time-dependent generalized pseudospectral method [37–39], in which the electron wave function is

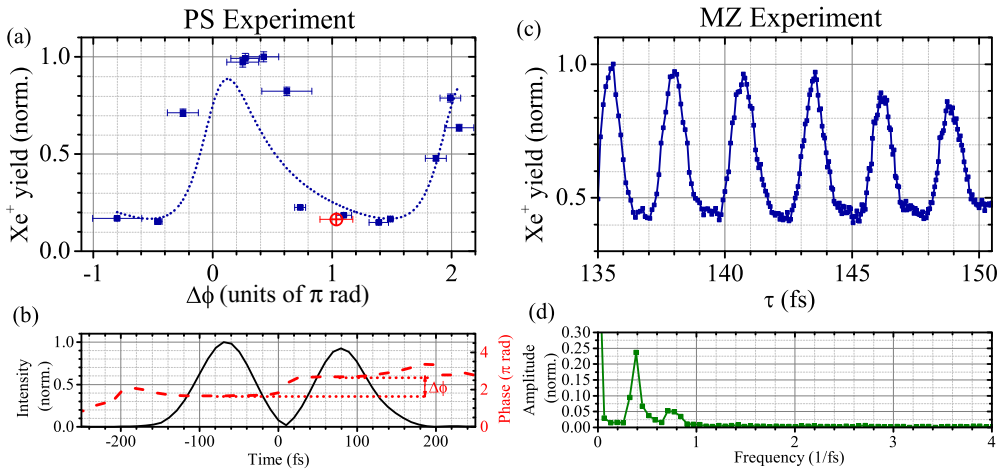

FIG. 1. The normalized measured phase-dependent Xe^+ signal summed over all Xe^+ isotopes, captured from 1000 TOF waveforms per point. (a) The yield induced by a TPP_{PS} at $\tau = 150$ fs. Maximal ion yield occurred between 0.2π and 0.4π rad. The dotted blue curve is the fit of the data to $Y = (I_{TPP}^{(max)})^{3/2}$, where the TPP maximum intensity $I_{TPP}^{(max)}$ is calculated for $T \equiv \tau/\Delta t = 3$ and assuming an input pulse with a pedestal, defined in Eq. (11) with $\beta = 0.23$ and $\phi_p = 1.17\pi$ rad (see text). (b) The FROG reconstructed intensity profile (solid black curve) and phase (dashed red curve) for the TPP_{PS} responsible for the red $\oplus$ datum point in panel (a), where $\Delta\phi \simeq \pi$ rad. (c) The Xe^+ signal vs τ from $\tau = 135$ to 150 fs, in steps of approximately 0.067 fs, induced by a TPP_{MZ}. The Fourier transform of panel (c) is shown in panel (d).

discretized on an optimized momentum grid (depending on a single-variable parameter) and propagated accurately using the split-operator scheme. The total ionization probability was calculated by projecting the postinteraction wave function onto the continuum states of the unperturbed Hamiltonian.

IV. RESULTS

Figure 1(a) shows an example of the Xe^+ phase-dependent ionization induced by a TPP_{PS} over a 3π-rad range for $\tau \simeq 150$ fs. The ion signal is normalized to its peak value and is the sum of all Xe^+ isotopes (in their natural abundances) in the captured TOF wave forms corresponding to 1000 laser shots. We refer to the location of the peak value of the ion signal as $\Delta\phi_0^{(E)}$. The three data points with the highest yield occur between 0.2π and 0.4π rad at the phase step resolution; thus we set $\Delta\phi_0^{(E)} = 0.3(1)\pi$ rad. Figure 1(b) displays a FROG-reconstructed intensity distribution of one TPP_{PS} corresponding to the red $\oplus$ datum point in Fig. 1(a). We see from this example of a TPP_{PS} that even well-separated peaks can reduce the yield substantially when they are π rad out of phase. Figure 1(c) shows a similar phase dependence at a higher resolution induced by a TPP_{MZ} for 135 fs $\leqslant \tau \leqslant$ 150 fs; the step size, $\delta\tau \simeq 0.067$ fs, corresponds to $\delta(\Delta\phi) \simeq \pi/20$ rad [see Eq. (2)]. The Fourier transform of Fig. 1(c) is shown in Fig. 1(d). Two frequencies dominate: 0.375 fs^{-1} (the optical frequency) and 0.75 fs^{-1} (twice the optical frequency). In Sec. I, we argued that a QuI contribution to the signal modulation can appear at frequencies ν_0, $7\nu_0$, or $8\nu_0$. No modulation greater than twice the optical frequency is observed above the noise.

The top panel of Fig. 2(a) shows the TPP_{MZ} spectrum for 50 fs $\leqslant \tau \leqslant$ 230 fs (top) with a resolution of $\delta\tau \simeq 0.67$ fs. The middle panel of Fig. 2(a) provides the peak values of Eq. (7), denoted $I_{sim}^{(max)}(\tau, \Delta\phi)$. Figure 2(c) shows $I(t)$ and $\phi(t)$ that were used in Eqs. (6) and (7) with $\lambda_0 = 810$ nm. The bottom panel of Fig. 2(a) presents the TDSE simulation of the ionization, also using the input pulse from Fig. 2(c), but for $\lambda_0 = 808$ nm. To facilitate comparison with Fig. 1(d), we show in Fig. 2(b) the Fourier transforms of the three spectra. We note again that there is a large uncertainty in the exact value of τ in the experiment, even though we know $\delta\tau$ well. This gives rise to an unknown phase shift in the top panel of Fig. 2(a) but does not affect our knowledge of the oscillation period.

V. DISCUSSION

The results displayed in Figs. 1 and 2 allow us to make five salient observations about strong-field ionization with phase-locked TPPs, having relevance to optimal control. While some responses we point out may be subtle, we argue below that these issues, which have largely been overlooked in efforts to decipher optimal control pulses, may play a more fundamental role than previously thought.

Two things are immediately obvious in Fig. 1(a). First, we see that even a minimal overlap of the peaks (about 10% in this case) is sufficient to induce significant modulation in the ionization signal strength. Evidently, OI must be taken into account even when pulse overlap occurs in the peak wings. Second, we note that the maximum ionization is between 0.2π and 0.4π rad ($\Delta\phi_0^{(E)}$) instead of at 0 rad, where one naively might expect to find these extrema if OI were the sole mechanism. The third observation we make is that only two frequencies appear in the Fourier transforms in Figs. 1(d) and 2(b), ν_0 and $2\nu_0$. While this frequency doubling is most noticeable in the lower two traces in Fig. 2(a) for 80 fs $\leqslant \tau \leqslant$ 180 fs, it is also observed for 100 fs $\leqslant \tau \leqslant$ 120 fs and 140 fs $\leqslant \tau \leqslant$ 160 fs in the top trace. The frequency doubling exhibits a phase slip with the stronger and weaker components switching near $\tau \simeq 100$ fs.

Most strong-field pulses have imperfections in their wings; our TPP_{MZ} is no exception. The nature of the imperfections

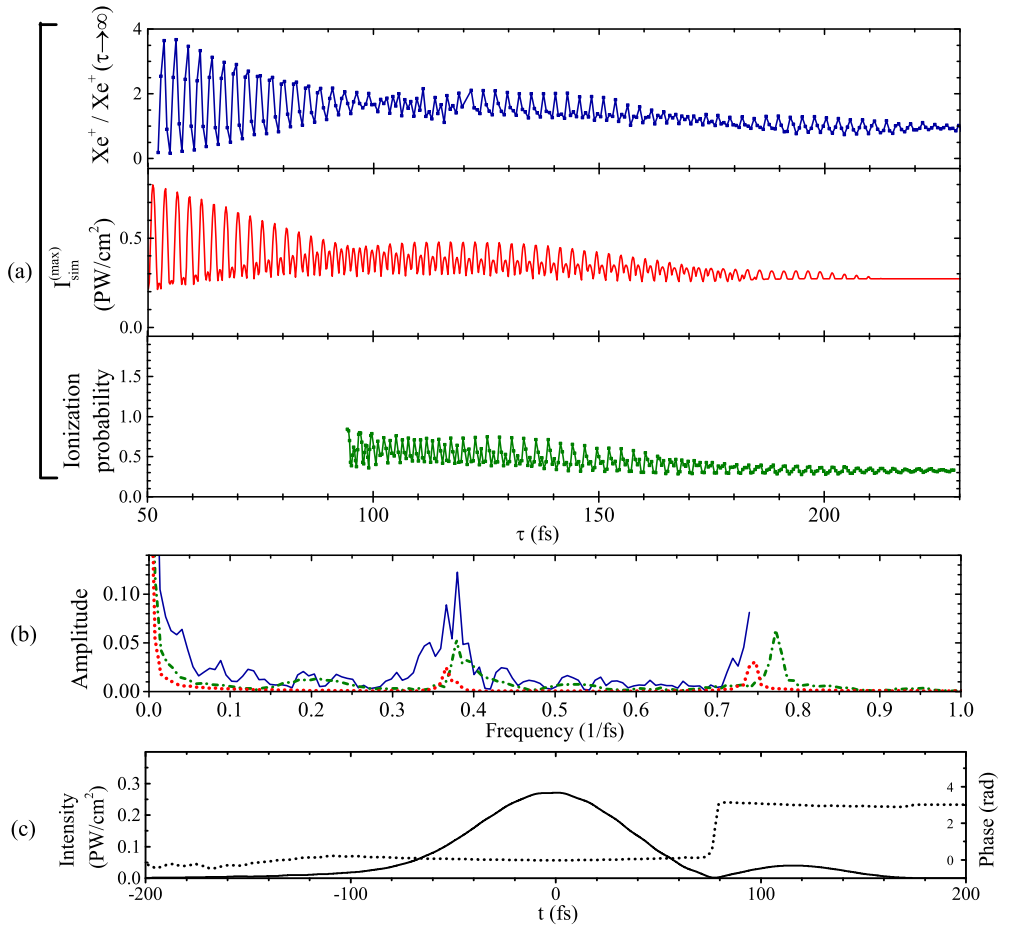

FIG. 2. (a) The top spectrum is the measured Xe^+ yield generated by a TPP_{MZ} vs τ, between 50 and 230 fs in steps of 0.67 fs. The yield is normalized to 1 when $\tau \gg \Delta t$. The middle spectrum is $I_{\rm sim}^{(\rm max)}$ from Eq. (7) with $\lambda_0 = 810$ nm. The bottom spectrum is the TDSE calculation with $\lambda_0 = 808$ nm described in Sec. III. The peaks of the top trace are shifted from the middle and bottom traces, but this is due to the large uncertainty in τ. The oscillation frequencies of the top trace are not affected due to the small uncertainty in $\delta\tau$, the relative delay between points. (b) The Fourier transforms of the spectra in panel (a): measured (solid blue curve), $I_{\rm sim}^{(\rm max)}$ (dotted red curve), and TDSE (dash-dotted green curve). (c) $I(t)$ (solid) and $\phi(t)$ (dotted) SD-FROG reconstructions for the input pulse used in the simulations.

is the fourth issue we point out here. Specifically, the input pulse [Fig. 2(c)] had a trailing shoulder (referred to as the subordinate peak) containing about 10% of the energy of the nearly transform-limited main peak. The phase of the subordinate peak differed from the main peak by about π rad. The subordinate peak was due to third-order spectral phase surviving compression. Our fifth observation concerns the nature of the modulations exhibited in the measured and simulated spectra in Fig. 2(a). All exhibit a fast modulation with a slower envelope. For 50 fs $\leqslant \tau \leqslant$ 100 fs both the measured yield and $I_{\rm sim}^{(\rm max)}(t)$ exhibit fast oscillation with contrasts that decrease monotonically. In the neighborhood of 100 fs, the modulation nearly vanishes in the measured spectrum. The measured spectrum is erratic between 100 and 120 fs, after which it revives briefly before decreasing monotonically again.

In the remainder of this section, we discuss in more detail OI-induced modulation of ionization in light of the five observations listed above. We use our data to set an upper bound to QuI under our conditions. Finally, we conclude the section with a discussion of the relevance of our findings to strong-field control.

A. OI-induced ionization modulation

The deceptively large contrast in Fig. 1(a) is due to enhancing the interference between the peaks caused by fixing the energy of the TPP. To explain this quantitatively, we look at the intrapeak OI for a TPP_{PS}. Particularly, we calculate the maximum intensity of an ideal $\rm sech^2$ TPP, denoted $I_{\rm TPP}^{(\rm max)}$. We distinguish this from $I_{\rm sim}^{(\rm max)}$, introduced in Sec. III, in that $I_{\rm sim}^{(\rm max)}$ was calculated numerically using an arbitrary pulse shape, while $I_{\rm TPP}^{(\rm max)}$ is calculated analytically from Eq. (4). For a fixed τ, $I_{\rm TPP}^{(\rm max)}$ will change as $\Delta\phi$ varies due only to OI between the two peaks, but depends on three factors as shown in Eq. (8), which is derived in the Supplemental Material [40]:

$$I_{\rm TPP}^{(\rm max)}(T,\Delta\phi) = I_0 f_{OI} f_{EC}, \tag{8}$$

where

$$f_{OI}(T,\Delta\phi) = 1 + \mathrm{sech}^2(T) + 2\mathrm{sech}(T)\cos(\Delta\phi) \tag{9}$$

is a modification factor due to intra-peak OI, and

$$f_{EC}(T,\Delta\phi) = \{1 + [T\,\mathrm{csch}(T)]\cos(\Delta\phi)\}^{-1} \tag{10}$$

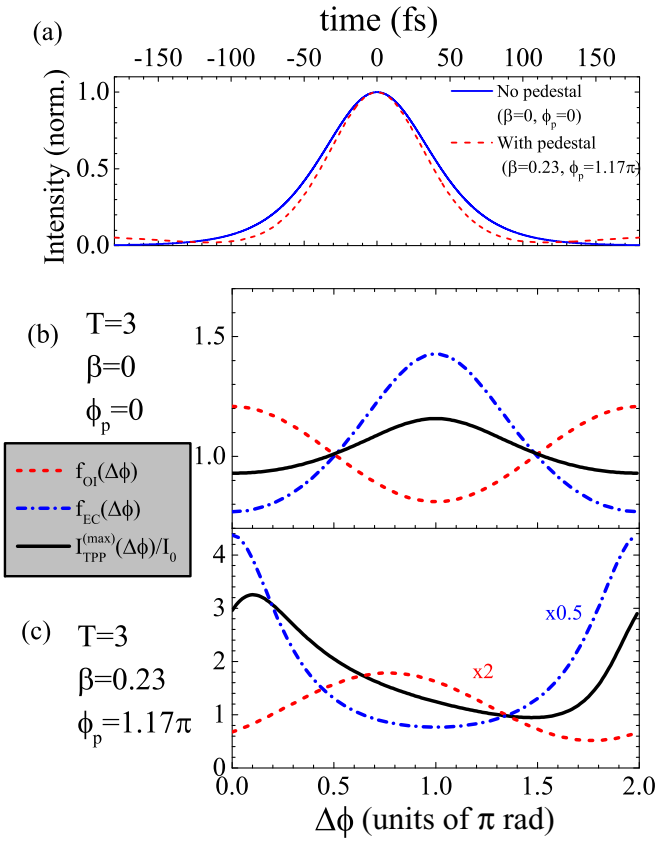

FIG. 3. (a) The temporal intensity profile of the model pulses: with (red dashed) and without (solid blue) a pedestal defined in Eq. (11) and $\beta = 0.23$, $\phi_p = 1.17\pi$ rad. (b) $I_{\rm TPP}^{(\rm max)}/I_0$ (solid black curve), f_{OI} (dashed red curve), and f_{EC} (dot-dashed blue curve) with no pedestal as a function of relative phase $\Delta\phi$, for $T \equiv \tau/\Delta t = 3$, which closely approximates the experimental $\rm TPP_{PS}$ parameters. (c) Same as panel (b) but with the pedestal. For ease of viewing, f_{OI} and f_{EC} have been multiplied by 2 and 0.5, respectively.

is an intended correction factor due to fixing the $\rm TPP_{PS}$ energy. Both factors depend on the ratio $T \equiv \tau/\Delta t$. Figure 3(b) shows how f_{OI} and f_{EC} vary with $\Delta\phi$ for the case of $T = 3$, which is the value extracted from our FROG measurements, and their influence on $I_{\rm TPP}^{(\rm max)}$. While f_{OI} and f_{EC} oscillate out of phase, they have different amplitudes—fixing the energy only partially eliminates OI-induced intensity fluctuations. There remains a variation in $I_{\rm TPP}^{(\rm max)}$ of about 10% of its average value. The peak value of $I_{\rm TPP}^{(\rm max)}$ occurs at $\Delta\phi_0^{(M)} = \pi$ rad, in contrast to 0.2π rad $\leqslant \Delta\phi_0^{(E)} \leqslant 0.4\pi$ rad in the ion signal. We defer the discussion of the origin of this phase shift to Sec. V B.

We note that to lowest order, the ion yield Y for a nonresonant, eight-photon ionization varies as $(I_{\rm TPP}^{(\rm max)})^8$ for a sufficiently weak field. At higher intensities, several factors can cause a different dependence. The first factor is a transition from the multiphoton to tunneling regime. At 3×10^{14} W/cm^2, our Keldysh parameter [7] is $\simeq$0.6, placing us in the tunneling regime [41]. Second, at high intensities, the corona of the pulse is a significant contributor to ionization, which can lead to a mixing of multiphoton and tunneling ionization, depending on where in the focus an atom is ionized. Eventually, this leads to $Y \propto (I_{\rm TPP}^{(\rm max)})^{3/2}$ at very high intensities [12,13], but space charge effects due to the corona are present at lower intensities as well [41]. Regardless, a power-law dependence $Y \propto (I_{\rm TPP}^{(\rm max)})^p$ is maintained. Our intensities imply that $p \simeq 3/2$ based on the results in Ref. [41]. We performed an unmasked intensity scan using a $\rm TPP_{MZ}$ with fixed τ and $\Delta\phi$, for intensities between 2.7 and 3.3 $\times 10^{14}$ W/cm^2, and found that $p = 1.2(1)$.

B. Phase shift of the OI response

As seen in Fig. 3(b), f_{OI} and f_{EC} oscillate out of phase with each other for an ideal TPP and peak at $\Delta\phi = 0$ and $\Delta\phi = \pi$ rad, respectively. The maximum intensity $I_{\rm TPP}^{(\rm max)}$ oscillates with either f_{OI} or f_{EC}, depending on if f_{OI} or f_{EC} has the larger magnitude, with the crossover occurring at $T = 1.6$ (the corresponding τ depends on the peak width Δt). For $T > 1.6$, $f_{OI} < f_{EC}$. In our PS experiment, $T \simeq 3$, which means that $\Delta\phi_0^{(M)} = \pi$ rad. Recall that the peak ion yield is observed between 0.2π and 0.4π rad.

The discrepancy between $\Delta\phi_0^{(M)}$ and $\Delta\phi_0^{(E)}$ has its origin in the fact that the experimental $\rm TPP_{PS}$ is not composed of ideal sech^2 peaks of equal amplitude. There are two categories of modifications of concern. First, there are modifications that change the relative intensities and widths of the two peaks but maintain a sech^2 peak shape—we refer to these as proportional modifications. The effects of proportional modifications can be probed by modifying the amplitudes and the widths of the peaks in Eq. (1). One finds, however, that proportional modifications do not change the locations of the peak values of f_{OI} and f_{EC}. As a result, proportional modifications will also not change $\Delta\phi_0^{(M)}$ for a given T. This would explain why even though we observe the relative intensities and widths of the peaks fluctuating by about 10%, the phase-dependent ionization yield modulation is robust.

The second class of modifications are pulse shape distortions, which change the shape of the individual peaks away from an ideal sech^2. Pulse shape distortions can be observed when we try to fit an ideal TPP to a FROG-reconstructed TPP, as can be seen in Fig. 4. In this figure, an experimentally measured $\rm TPP_{PS}$ [$\Delta\phi \simeq \pi$ rad, same TPP as in Fig. 1(b)] was fit to Eq. (4), where the heights and widths of the two peaks were allowed to differ. While the deviations between fit and experiment are small, it is straightforward to show that even a small pulse shape distortion will change $\Delta\phi_0^{(M)}$. To show that $\Delta\phi_0^{(M)}$ is sensitive to pulse shape distortions, we created a "toy" distortion model consisting of adding a symmetric pedestal to the peaks. We represented the pedestal by a rectangular function, with a width of $10\Delta t$. The field of an input pulse with the pedestal is

$$\mathcal{E}(t) = \mathcal{E}_0 e^{-i(\omega_0 t-\phi_1)}\left[\operatorname{sech}\left(\frac{t}{\Delta t}\right) + \beta\Pi\left(\frac{t}{10\Delta t}\right)e^{i\phi_p}\right] + \text{c.c.}, \tag{11}$$

where ϕ_p is the relative phase between the pedestal and the main peak, β is the ratio of the field amplitude of the pedestal to that of the main peak, and

$$\Pi\left(\frac{t}{10\Delta t}\right) = \begin{cases} 1, & |t| \leqslant 5\Delta t, \\ 0, & |t| > 5\Delta t. \end{cases} \tag{12}$$

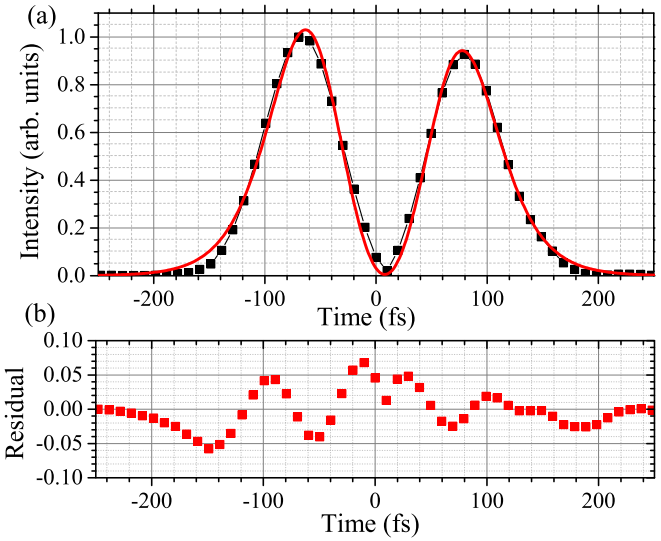

FIG. 4. (upper) Temporal intensity of a FROG-reconstructed TPP_{PS} [black squares, same TPP as Fig. 1(b)] and a fit of of this TPP to a model hyperbolic-secant TPP with $\Delta\phi = 1.04\pi$ rad (red curve). The fit is to Eq. (4) with proportional modulations added; i.e., the heights and widths of the two peaks were allowed to differ. The fit recovers widths for the first and second peaks, respectively, of $\Delta t_1 = 49.0(7)$ and $\Delta t_2 = 48.7(8)$ fs, and amplitudes $I_{01} = 1.35(2)$ and $I_{02} = 1.27(2)$. (lower) Residual of the fit shown in the upper panel (data minus fit curve).

After defining the input pulse with Eq. (11), we recalculated $f_{OI}(T,\Delta\phi)$, $f_{EC}(T,\Delta\phi)$, and $I_{\rm TPP}^{(\rm max)}(T,\Delta\phi)$. This calculation is shown in the Supplemental Material [40]; it is important to recognize that ϕ_p causes a phase shift in both f_{OI} and f_{EC}. Next, we fit the data in Fig. 1(a) to $Y \propto (I_{\rm TPP}^{(\rm max)})^{3/2}$, allowing ϕ_p and β to vary, and fixing $T = 3$. The dotted curve in Fig. 1(a) shows the result of the fit, using the fit values $\phi_p = 1.17(5)\pi$ rad and $\beta = 0.23(2)$.

The effect of this pedestal on $I_{\rm TPP}^{(\rm max)}$ is shown in Fig. 3(c). With such a pedestal added, $\Delta\phi_0^{(M)} \simeq 0.1\pi$ rad, which is only one standard deviation outside the range of 0.2π rad $\leqslant \Delta\phi_0^{(E)} \leqslant 0.4\pi$ rad. The variation in $I_{\rm TPP}^{(\rm max)}$ is much larger than in the case without a pedestal, which is necessary to reproduce the large ion yield contrast seen in the experiment. Input pulses with and without this pedestal are compared in Fig. 3(a), showing that the addition of the pedestal reduces the intensity in the wings of the pulse. We point out the fact that the PS pulse was shaped with an input similar to that shown in Fig. 2(c) so it should not be surprising that the PS spectrum has a pedestal. The MZ spectra probably also have a phase shift, but due to the large uncertainty in determining τ this phase shift was not determined. We also point out that $I_{\rm TPP}^{(\rm max)}$ was calculated in this toy model by evaluating $I_{\rm TPP}$ at $t = 0$, i.e., finding the maximum intensity of the earlier peak. When a pedestal is present, the intensity of the second peak does not follow the intensity of the first peak, and so the intensity at $t = 0$ is not necessarily $I_{\rm TPP}^{(\rm max)}$. We stress that the intent of this toy model was to show that *some* phase shift can be added to the $I_{\rm TPP}^{(\rm max)}$ by the introduction of a pulse shape distortion, which has been shown to be the case here.

C. Slow envelope modulation

The slowly varying temporal envelope observed in the three spectra in Fig. 2(a) roughly follow the temporal shape of the input pulse. For $\tau < 100$ fs, the overlaps of the two main peaks of the TPP_{MZ} dominates OI, so the modulation contrast is set by the temporal shape of the main peaks. Each peak of the TPP_{MZ} carries the character of Fig. 2(c). Consequently, the revival of the modulation for $\tau > 100$ fs is due to OI between a main and subordinate peak. The envelope of modulation is now given by a convolution of the two temporal shapes. While there was a secondary revival of the oscillation envelope in the experimental ion yield plot for $\tau > 180$ fs, we believe this is due to a sample rate artifact due to our large τ step size of 0.67 fs.

D. Frequency doubling

The modulation at the optical frequency ν_0 is well described by OI; here we focus on the oscillations at frequency $2\nu_0$. While this frequency doubling could be due to two-photon QuI mechanism I, similar to what is described in Ref. [30], there are several reasons why this is unlikely. First, there are no two-photon intermediate states that can be reached from the ground state at 800 nm. The first excited state in xenon requires more than five 800-nm photons to reach. Second, $I_{\rm sim}^{(\rm max)}$ and its Fourier transform (Fig. 2) show the same frequency doubling as the TPP_{MZ} spectra. The $I_{\rm sim}^{(\rm max)}$ spectrum was calculated using OI alone. Consequently, the frequency doubling it exhibits can only be caused by OI.

The most likely origin of the frequency doubling is the subordinate peak via OI. The subordinate peak in the input pulse [Fig. 2(c)] was π rad out of phase with the main peak. Consider a TPP_{MZ} with 100 fs $\leqslant \tau \leqslant$ 150 fs, and $\Delta\phi = 0$. In this case, the intensity of the earlier main peak will increase due to constructive OI. At the same time, the intensity of the later main peak will decrease due to destructive OI with the earlier subordinate peak. So, the earlier peak intensity will be larger than the later peak intensity. Conversely, if $\Delta\phi = \pi$ rad, the later peak intensity will be larger than the earlier peak intensity. This switching back and forth of intensities is what leads to the frequency doubling when 100 fs $\leqslant \tau \leqslant$ 150 fs. For a video of OI vs τ that illustrates these statements, see the Supplemental Material [40].

E. Upper bound to QuI strength

We find in the PS and MZ experiments that the change in maximum intensity of a TPP due to OI is principally responsible for the fluctuations in ionization yield. Neither experiment showed any definitive evidence of QuI mechanism III. The null result in this search for QuI allows us to estimate the maximum size of the QuI-induced oscillations. We note that the QuI oscillation amplitude must be larger than the noise present in the data. In the MZ Fourier transform data shown in Fig. 1(d), we estimated the noise in the normalized yield to be approximately 0.025 (one can see this in the figure by looking at the troughs of each oscillation, particularly around $\tau =$ 145 fs). The OI oscillation amplitude averaged out to about 0.25 over the range shown [see Fig. 1(d)]. This puts an upper limit of the QuI amplitude at 10% of the OI amplitude. This rough 10% limit was found to apply at other values of τ as well.

There is perhaps a stronger reason we do not see QuI in our experiment. Quantum interference as we have described it can be considered a temporal analogue of a Young's double-slit experiment, with the two peaks of the TPP representing the two slits and the TOF detector representing the screen. Under this analogy, the slit spacing is represented by the TPP relative phase $\Delta\phi$ (directly in the PS experiments and indirectly, through τ, in the MZ experiments). Ionization of an electron corresponds to a photon or massive particle passing through the double-slit apparatus. As with the double slit, there is an ambiguity as to which peak was responsible for producing the electron. In a traditional double-slit experiment, the particles pile up on the screen at different locations with the minima and maxima determined by the relative phase after passing through the slits. The analogue in our case is where the electrons land. We, however, are not measuring the electrons, but rather the ions. Measuring the ions is equivalent to integrating all of the photons or particles that land on the screen. The total number of photons or particles just depends on the throughput of the slit, not on the interference. Consequently, we do not expect to see QuI by just detecting the ions.

It is important to note that the insensitivity of the ion spectrum to QuI strictly holds only for transitions to an open channel (mechanism III). In Ref. [30], modulation of the total ion yield due to QuI is observed and clearly differentiated from OI, because in that case QuI was mediated by mechanisms I and II, via transitions to bound states. In an open-channel experiment, like that done in Ref. [31] and here, the Young's double-slit analogy suggests that modulation in the ion yield induced by QuI mechanism III will not occur, because we sum all the electrons and, thus, lose differential information contained in the photoelectron spectrum. While the total electron yield is seen to change with changing TPP relative phase in Ref. [31], it only does so when the two peaks of the TPPs are very closely separated, so OI was likely making a substantial contribution to what was observed. However, QuI could still appear in an open channel experiment via mechanisms I and II involving intermediate states.

Rather than a measurement of the total electron or ion yield, an energy-resolved photoelectron measurement would be necessary to see evidence of QuI mechanism III. The energy of a photoelectron is connected to the location of a particle on the screen in our double-slit analogy, so an energy-resolved measurement is akin to recording the interference pattern on the screen rather than counting up all particles. It would be desirable to perform an energy-resolved experiment with TPPs which probes a multiphoton transition to the ionic continuum, which would allow for a clear differentiation between OI and QuI. While rotating the polarization of one of the peaks of the TPP to eliminate OI is also a possibility, this is not ideal because the angular distribution may have limited overlap. Selection rules may cause the two peaks to ionize to two different sets of final states, in which case the quantum interference will break down as there is full knowledge of which peak produced the photoelectron.

F. Relevance to strong-field control

A common theme emerges from our discussion of the experiments. Small, subtle changes in the pulse shape can affect the OI substantially, and, subsequently, affect the ionization. This realization has direct application to optimal control in the strong-field regime. As previously mentioned, ionization usually occurs in strong-field optimal control experiments. While the discussion of how an optimal control pulse guides a target system to its final state typically focuses on dominant features of the pulse (e.g., peak widths, delay between successive peaks, chirp, etc.), we now have evidence that more subtle features (e.g., relative phase between peaks, small structure and imperfections, etc.) can influence the control process just as dramatically.

We consider here one specific example, using our previous work on controlling CO_2 bending vibration during strong-field dissociative-ionization [15]. In Fig. 2 of Ref. [15], two optimal control pulses for maximizing the bending vibration amplitude during dissociation are shown, along with the phase-reversed pulses [where all other spectral parameters were the same except $\phi(\omega) \rightarrow -\phi(\omega)$]. Both optimal control pulses consist of a sequence of peaks with well-defined relative phases between the ith and jth peaks of an optimal control pulse $\Delta\phi_{ij}$. For the phase-reversed pulses, $\Delta\phi_{ij} \rightarrow -\Delta\phi_{ij}$. It was found that the two optimal control pulses significantly enhanced the bending amplitude when compared with either a transform-limited pulse at the same intensity or their respective phase-reversed pulses.

In Sec. V B, we saw that a weak pedestal, as a model for symmetric distortion of an ideal shape, significantly changed OI between a pair of pulses; with such a pedestal, two pulses with a relative phase $\Delta\phi$ did not have the same peak intensity as two pulses with a relative phase of $-\Delta\phi$ in general. As such, the presence of a pedestal would imply that the optimal control pulse and its phase-reversed counterpart did not necessarily have the same peak intensity (even if their energies were the same). Because the CO_2 bending vibration amplitude depends strongly on the pulse intensity for transform limited pulses (see Fig. 3 of Ref. [15]), these two pulses would have produced different amounts of CO_2 bending vibration. A pedestal is unlikely to have been the only "knob" with which the bending vibration was controlled; however, it highlights the need to consider purely optical effects carefully, alongside the field-system dynamics, when discussing strong-field optimal control experiments. This example also highlights an advantage learning algorithm-based optimal control experiments have over manual manipulation—the learning algorithm can access regions of the control landscape (in this example, the pulse distortions) that are not easily accessible *a priori*.

VI. CONCLUSION

By measuring, both in theory and experiment, the ionization response to TPPs, we have arrived at two main conclusions. First, we have demonstrated that the ion yield can be predicted by considering the maximum intensity of the pulse due to OI under the conditions of our experiment. While QuI (only mechanisms I and II) could influence the ion yield to a degree, any contributions are overshadowed by the noise in our experiment, and we place a rough limit on the strength of QuI at 10% of the strength of OI around $\tau = 150$ fs. An energy-resolved measurement like that done in Ref. [31] should be able to see dynamics induced by QuI mechanism III in

multiphoton ionization. The temporal and/or phase resolution of the experiment must be high enough to resolve oscillations at frequency $n\nu_0$, where n is the multiphoton order. The current MZ experiment is of sufficient temporal resolution, but a higher resolution pulse shaper is necessary in the PS experiments.

Second, our results also highlight that small changes in pulse parameters (such as pedestals, subordinate peaks, etc.) can lead to large changes in the TPP maximum intensity and resultant ionization yields, even when the pulses appear well separated. This is true whether or not the total pulse energy is fixed. These small pulse features can cause the OI to mimic the effects of QuI in some cases (e.g., by introducing frequency doubling). Most strong-field experiments that seek to control molecular and chemical dynamics use ionization as a first step, and so any final system dynamics will be sensitive to intensity fluctuations of the pulses as well, as seen in Ref. [15] for example.

ACKNOWLEDGMENTS

The experimental work at the University of Maryland was supported by NSF Grant No. PHY1506332. The work at the University of Nebraska was supported in part by NSF Grant No. PHYS-1505492 [L.W.P. and A.F.S.] and by NSF EPSCoR IRR Track II Research Award No. 1430519 [J.M.N.D.]. The authors thank F. Robicheaux [W.T.H.] and C. Clark [D.B.F. and W.T.H.] for helpful discussions.

[1] R. J. Levis and H. A. Rabitz, J. Phys. Chem. A **106**, 6427 (2002).
[2] H. Rabitz, Science **299**, 525 (2003).
[3] H. Rabitz, Science **314**, 264 (2006).
[4] P. Lambropoulos, in *Topics on Multiphoton Processes in Atoms*, Advances in Atomic and Molecular Physics, edited by D. Bates and B. Bederson (Academic Press, San Diego, CA, 1976), Vol. 12, pp. 87–164.
[5] P. Lambropoulos, Phys. Rev. Lett. **55**, 2141 (1985).
[6] L. Pan, B. Sundaram, and L. Armstrong, J. Opt. Soc. Am. B **4**, 754 (1987).
[7] L. V. Keldysh, Zh. Eksp. Teor. Fiz. **47**, 1945 (1965) [Sov. Phys. JETP **20**, 1307 (1965)].
[8] M. V. Ammosov, N. B. Delone, and V. P. Krainov, Zh. Eksp. Teor. Fiz. **91**, 2008 (1986) [Sov. Phys. JETP **64**, 1191 (1986)].
[9] S. V. Popruzhenko, J. Phys. B **47**, 204001 (2014).
[10] G. N. Gibson, R. R. Freeman, T. J. McIlrath, and H. G. Muller, Phys. Rev. A **49**, 3870 (1994).
[11] T. Marchenko, H. G. Muller, K. J. Schafer, and M. J. J. Vrakking, J. Phys. B **43**, 185001 (2010).
[12] S. Speiser and J. Jortner, Chem. Phys. Lett. **44**, 399 (1976).
[13] J. Strohaber and C. J. G. J. Uiterwaal, Phys. Rev. Lett. **100**, 023002 (2008).
[14] W. D. M. Lunden, P. Sándor, T. C. Weinacht, and T. Rozgonyi, Phys. Rev. A **89**, 053403 (2014).
[15] G.-Y. Chen, Z. W. Wang, and W. T. Hill, III, Phys. Rev. A **79**, 011401(R) (2009).
[16] M. Wollenhaupt, M. Krug, J. Köhler, T. Bayer, C. Sarpe-Tudoran, and T. Baumert, Appl. Phys. B **95**, 245 (2009).
[17] P. Hockett, M. Wollenhaupt, and T. Baumert, J. Phys. B **48**, 214004 (2015).
[18] N. Kanda, T. Higuchi, H. Shimizu, K. Konishi, K. Yoshioka, and M. Kuwata-Gonokami, Nat. Commun. **2**, 362 (2011).
[19] V. Nikiforov, A. Shmelev, G. Safiullin, and V. Lobkov, Chem. Phys. Lett. **592**, 196 (2014).
[20] T. Hornung, R. Meier, R. de Vivie-Riedle, and M. Motzkus, Chem. Phys. **267**, 261 (2001).
[21] T. Hornung, R. Meier, and M. Motzkus, Chem. Phys. Lett. **326**, 445 (2000).
[22] E. Papastathopoulos, M. Strehle, and G. Gerber, Chem. Phys. Lett. **408**, 65 (2005).
[23] N. X. Truong, P. Hilse, S. Göde, A. Przystawik, T. Döppner, T. Fennel, T. Bornath, J. Tiggesbäumker, M. Schlanges, G. Gerber, and K. H. Meiwes-Broer, Phys. Rev. A **81**, 013201 (2010).
[24] F. Langhojer, D. Cardoza, M. Baertschy, and T. Weinacht, J. Chem. Phys. **122**, 014102 (2005).
[25] T. Bayer, M. Wollenhaupt, and T. Baumert, J. Phys. B: At. Mol. Opt. Phys. **41**, 074007 (2008).
[26] V. V. Lozovoy, X. Zhu, T. C. Gunaratne, D. A. Harris, J. C. Shane, and M. Dantus, J. Phys. Chem. A **112**, 3789 (2008).
[27] N. Schirmel, N. Reusch, P. Horsch, and K.-M. Weitzel, Faraday Discuss. **163**, 461 (2013).
[28] M. Born and E. Wolf, *Principles of Optics*, 4th ed. (Pergamon Press, Oxford, UK, 1970).
[29] I. A. Walmsley and C. Dorrer, Adv. Opt. Photon. **1**, 308 (2009).
[30] V. Blanchet, C. Nicole, M.-A. Bouchene, and B. Girard, Phys. Rev. Lett. **78**, 2716 (1997).
[31] M. Wollenhaupt, A. Assion, D. Liese, C. Sarpe-Tudoran, T. Baumert, S. Zamith, M. A. Bouchene, B. Girard, A. Flettner, U. Weichmann, and G. Gerber, Phys. Rev. Lett. **89**, 173001 (2002).
[32] R. Trebino, K. W. DeLong, D. N. Fittinghoff, J. N. Sweetser, M. A. Krumbügel, B. A. Richman, and D. J. Kane, Rev. Sci. Instrum. **68**, 3277 (1997).
[33] T. Oksenhendler, S. Coudreau, N. Forget, V. Crozatier, S. Grabielle, R. Herzog, O. Gobert, and D. Kaplan, Appl. Phys. B **99**, 7 (2010).
[34] A. M. Weiner, J. P. Heritage, and E. M. Kirschner, J. Opt. Soc. Am. B **5**, 1563 (1988).
[35] Cambridge Research and Instrumentation SLM-128.
[36] K. Zhao, T. Colvin, W. T. Hill, III, and G. Zhang, Rev. Sci. Instr. **73**, 3044 (2002).
[37] T. Jiang, Comput. Phys. Commun. **178**, 571 (2008).
[38] Z. Zhou and S.-I. Chu, Phys. Rev. A **83**, 013405 (2011).
[39] T.-F. Jiang, S.-D. Jheng, Y.-M. Lee, and Z.-Y. Su, Phys. Rev. E **86**, 066702 (2012).
[40] See Supplemental Material at http://link.aps.org/supplemental/10.1103/PhysRevA.96.023425 for a derivation of the TPP maximum intensity for two cases, with and without a pedestal. The Supplemental Material also contains a video that tracks the temporal intensity of a TPP as the intrapeak delay is changed, showing how a complicated OI can produce a frequency-doubling effect.
[41] S. Larochelle, A. Talebpour, and S. L. Chin, J. Phys. B **31**, 1201 (1998).